

Experimental Section

Materials

$\text{SnCl}_4 \cdot 5\text{H}_2\text{O}$ ($\geq 98.0\%$), thioacetamide ($\geq 99.0\%$), $\text{Fe}_2(\text{SO}_4)_3$ ($\geq 99.0\%$), Na_2SO_4 ($\geq 99.0\%$), NaNO_3 ($\geq 99.0\%$), $\text{C}_7\text{H}_6\text{O}_3$ ($\geq 99.5\%$), $\text{KNaC}_4\text{H}_{12}\text{O}_{10} \cdot 4\text{H}_2\text{O}$ ($\geq 99.9\%$), NaOH ($\geq 96\%$), NaClO (≥ 99.9 wt %), NaNO_2 ($\geq 99.0\%$), NH_4Cl ($\geq 99.5\%$), $\text{C}_{12}\text{H}_{14}\text{N}_2 \cdot 2\text{HCl}$ ($\geq 99.0\%$), $\text{C}_6\text{H}_8\text{N}_2\text{O}_2\text{S}$ ($\geq 99.5\%$) were provided from Sigma-Aldrich Chemical Reagent Co., Ltd. and Sinopharm Chemical Reagent Co., Ltd. All of the reagents were of analytical grade and were used as received without further purification.

Synthesis of Fe-SnS₂ nanosheets

In brief, a piece of carbon cloth (CC, 2 cm×4 cm) was ultrasonically treated in concentrated HCl for 2 h, and cleaned with ethanol and distilled water several times. Then, 0.18 mM of thioacetamide and 0.09 mM of $\text{SnCl}_4 \cdot 5\text{H}_2\text{O}$ were dissolved in 30 mL of deionized water under stirring for 10 min, followed by addition of 0.0045 mM of $\text{Fe}_2(\text{SO}_4)_3$ under stirring for another 10 min. The mixed solution was transferred into a Teflon-lined stainless-steel autoclave, followed by immersing the pretreated CC in the solution. The autoclave was sealed and maintained at 180 °C for 12 h. After cooling to room temperature, the obtained Fe-SnS₂/CC was washed with deionized water and ethanol several times, and dried at 60 °C overnight. For comparison, the pristine SnS₂/CC was prepared by the same procedure without addition of $\text{Fe}_2(\text{SO}_4)_3$.

Electrochemical experiments

A CHI 660E electrochemical workstation (Chenhua, Shanghai) was utilized to operate electrochemical testing, which was performed in an H-shaped cell separated by Nafion 117 membrane. The prepared Fe-SnS₂/CC, saturated Hg/HgO, and platinum foil (1 × 1 cm²) were employed as the working electrode, reference electrode, and counter electrode, respectively. All potentials reported in this work were converted to reversible hydrogen electrode (RHE) scale by $E_{(\text{RHE})} = E_{(\text{Hg}/\text{HgO})} + (0.098 + 0.0591 \times \text{pH})$ and current densities were normalized to the geometric surface area. The area of the working electrode immerse in electrolyte is 1 cm². Linear sweep voltammetry (LSV) tests were performed at the rate of 10 mV s⁻¹ from 0.2 to -1.0 V

vs. RHE. The whole experiment was performed under ambient conditions.

Determination of NH₃

The produced NH₃ was determined by the indophenol blue method¹. Specifically, 0.5 mL of electrolyte was removed from the electrochemical reaction vessel and diluted 10 times with deionized water. The diluted solution (2 mL) was moved into a clean vessel followed by sequentially adding NaOH solution (2 mL, 1 M) containing C₇H₆O₃ (5 wt.%) and C₆H₅Na₃O₇ (5 wt.%), NaClO (1 mL, 0.05 M), and C₅FeN₆Na₂O (0.2 mL, 1wt.%) aqueous solution. After the incubation for 2 h at room temperature, the mixture was subjected to UV-vis measurements and resulted in the absorption spectrum (ranged from 500-800 nm). The absorption peak at 655 nm was ascribed to the generated indophenol blue originated from NH₃ in the target solution. The concentration-absorbance curves were calibrated by the standard NH₄Cl solution with a series of concentrations (Fig. S1, $y = 0.360x + 0.077$, $R^2 = 0.999$). The yield rate of NH₃ is calculated by the following equation²:

$$\text{NH}_3 \text{ yield} = (c \times V) / (17 \times t \times A) \quad (1)$$

Faradaic efficiency was calculated by the following equation:

$$\text{FE} = (n \times F \times c \times V) / (17 \times Q) \times 100\% \quad (2)$$

where c ($\mu\text{g mL}^{-1}$) is the measured NH₃ concentration, V (mL) is the volume of electrolyte in the cathode chamber (30 mL), t (s) is the electrolysis time and A is the surface area of CC ($1 \times 1 \text{ cm}^2$), n is the number of transferred electrons from NO₃⁻ to NH₃, F (96500 C mol^{-1}) is the Faraday constant, Q (C) is the total quantity of applied electricity.

Determination of NO₂⁻

NO₂⁻ in electrolyte was determined by a Griess test³. 0.5 mL of electrolyte was removed from the electrochemical reaction vessel and diluted 50 times with deionized water. Coloring solution was prepared by dissolving N-(1-naphthyl) ethylenediamine dihydrochloride (0.1 g), sulfonamide (1.0 g) and H₃PO₄ (2.94 mL, 85%) into 50 ml of DI water. 0.1 ml coloring solution were added to the diluted electrolyte. After the incubation for 20 min at room temperature, the mixture was subjected to UV-vis measurements and resulted in the absorption spectrum (ranged from 400-700 nm).

The absorbance at 540 nm was measured to determine the concentration of generated NO_2^- with a standard curve of NO_2^- (Fig. S2, $y = 0.507x + 0.013$, $R^2 = 0.999$).

Determination of N_2H_4

The Watt and Chrisp method⁴ was used to determine the concentration of N_2H_4 . 5 mL of electrolyte was removed from the electrochemical reaction vessel. The 330 mL of color reagent containing 300 mL of $\text{C}_2\text{H}_5\text{OH}$, 5.99 g of $\text{C}_9\text{H}_{11}\text{NO}$ and 30 mL of HCl were prepared as chromomeric reagent. Then, 5 mL of color reagent was added into 5 mL of prepared chromomeric reagent. After stirring for 15 min, the absorbance at 455 nm was measured to quantify the N_2H_4 concentration with a standard curve of hydrazine (Fig. S3, $y = 0.530x + 0.032$, $R^2 = 0.999$).

Characterizations

X-ray diffraction (XRD) pattern was acquired by a Rigaku D/max 2400 diffractometer. Scanning electron microscopy (SEM) was carried out on a JSM-6701 microscope. Transmission electron microscopy (TEM) and high-resolution transmission electron microscopy (HRTEM) were performed on a Tecnai G2 F20 microscope. The absorbance data of spectrophotometer was measured on MAPADA ULM 1912006 UV-vis spectrophotometer. X-ray photoelectron spectroscopy (XPS) analysis was performed on a PHI 5702 spectrometer. ^1H nuclear magnetic resonance (NMR) measurements were performed on a 500 MHz Bruker superconducting-magnet NMR spectrometer. Electron paramagnetic resonance (EPR) measurements were performed on a Bruker ESP-300 spectrometer.

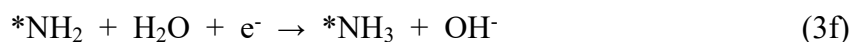
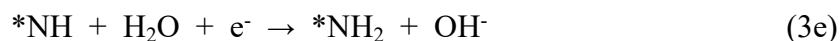
Nuclear magnetic resonance measurement

^1H nuclear magnetic resonance (NMR) measurements were carried out to confirm the origin of ammonium. After chronoamperometry tests in Ar-saturated 0.1 M NaOH with 0.1 M $^{14}\text{NO}_3^-$ at -0.8 V vs. RHE for 1 h, the pH of the post-electrolysis electrolyte was adjusted to 2 with 0.5 M HCl . Then, 0.05 mL of D_2O were added into 0.5 mL of above electrolyte for further ^1H NMR detection. The isotopic labeling experiment was conducted using Ar-saturated 0.1 M NaOH with 0.1 M $^{15}\text{NO}_3^-$ as the electrolyte in the same operation described above.

Calculation details

Spin-polarized density functional theory (DFT) calculations were carried out using a Cambridge sequential total energy package (CASTEP). The Perdew-Burke-Ernzerhof (PBE) generalized gradient approximation (GGA) functional was used for the exchange-correlation potential. The DFT-D correction method was considered for van der Waals forces. During the geometry optimization, the convergence tolerance was set to be 1.0×10^{-5} eV for energy and 0.02 eV \AA^{-1} for force. The Brillouin zone was sampled in a $4 \times 4 \times 1$ mesh. The electron wave functions were expanded using plane waves with a cutoff energy of 500 eV. The SnS₂ (001) was modeled by a 4×4 supercell, and a vacuum region of 15 \AA was used to separate adjacent slabs.

The NO₃ reduction reaction on the catalysts surfaces was simulated according to the following reactions⁵:



Where * represent the adsorption site, the free energies (ΔG , 298 K) for each reaction were given after correction⁶:

$$\Delta G = \Delta E + \Delta \text{ZPE} - T\Delta S \quad (4)$$

where ΔE is the adsorption energy, ΔZPE is the zero-point energy difference and $T\Delta S$ is the entropy difference between the gas phase and adsorbed state.

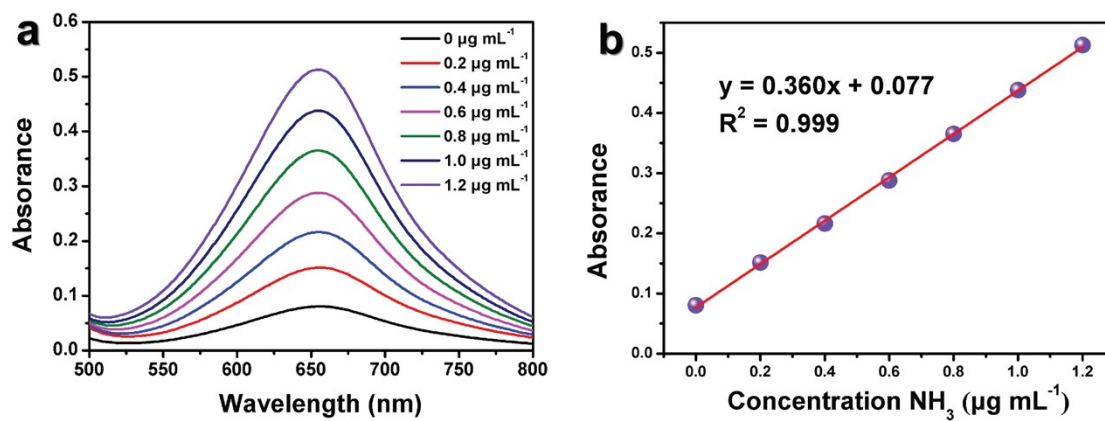


Fig. S1. (a) UV-vis absorption spectra and (b) corresponding calibration curve used for calculation of NH_3 concentrations.

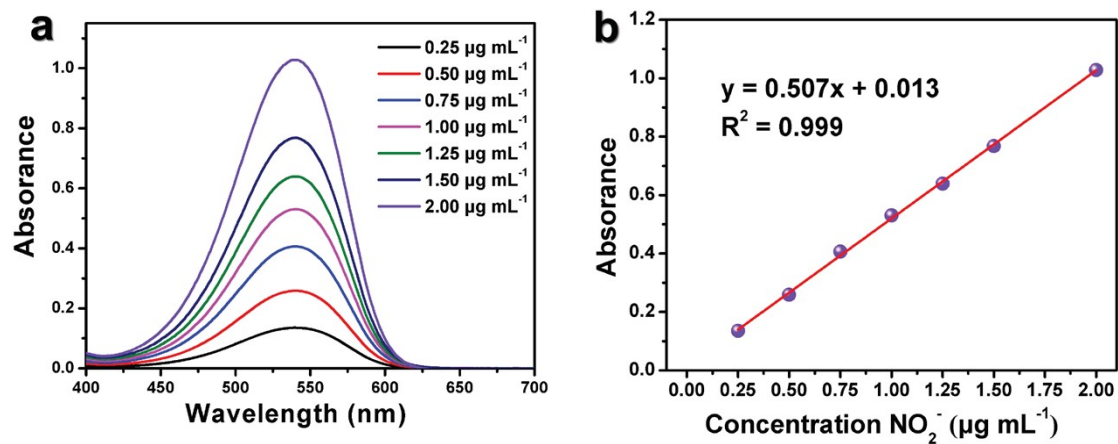


Fig. S2. (a) UV-vis absorption spectra (b) corresponding calibration curve used for calculation of NO_2^- concentrations.

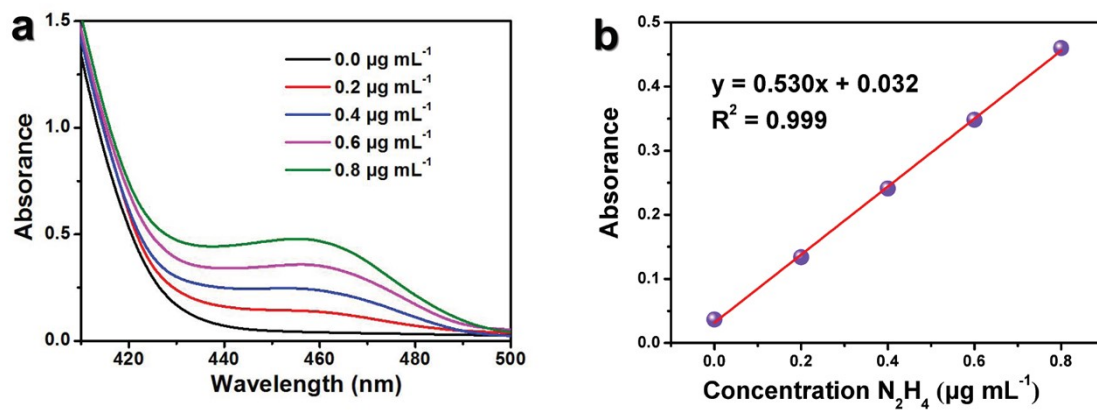


Fig. S3. (a) UV-vis absorption spectra and (b) corresponding calibration curve used for calculation of N_2H_4 concentrations.

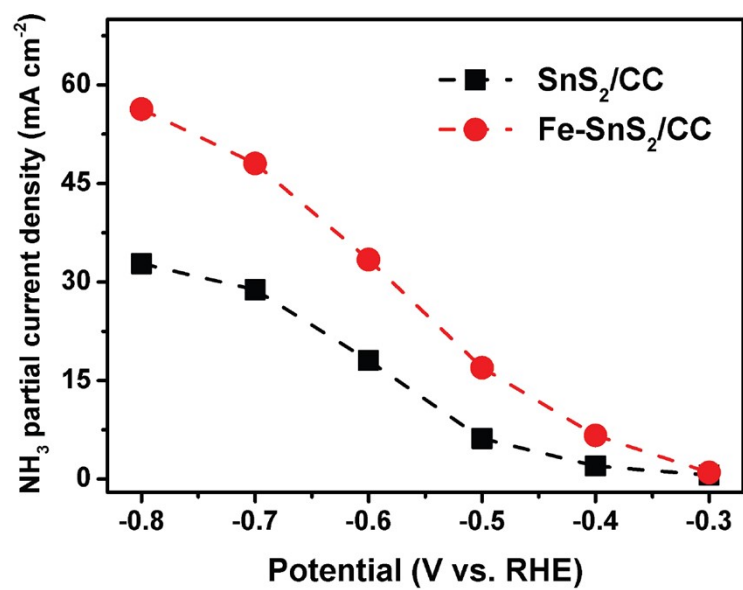


Fig. S4. NH₃ partial current densities of SnS₂/CC and Fe-SnS₂/CC.

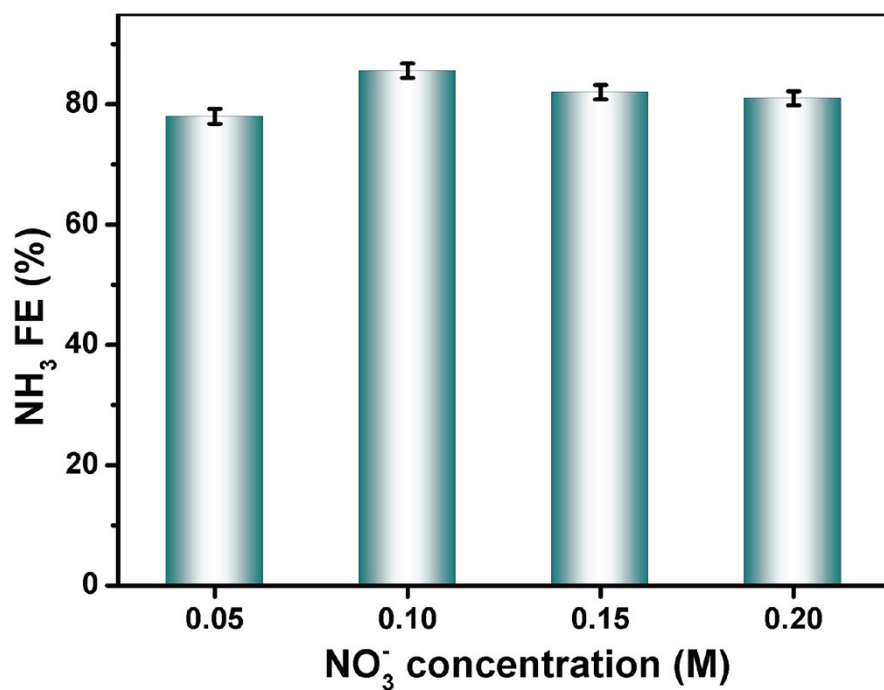


Fig. S5. The concentration of NO_3^- -N, NH_3 -N and NO_2^- -N in the electrolyte during the electrolysis at -0.7 V.

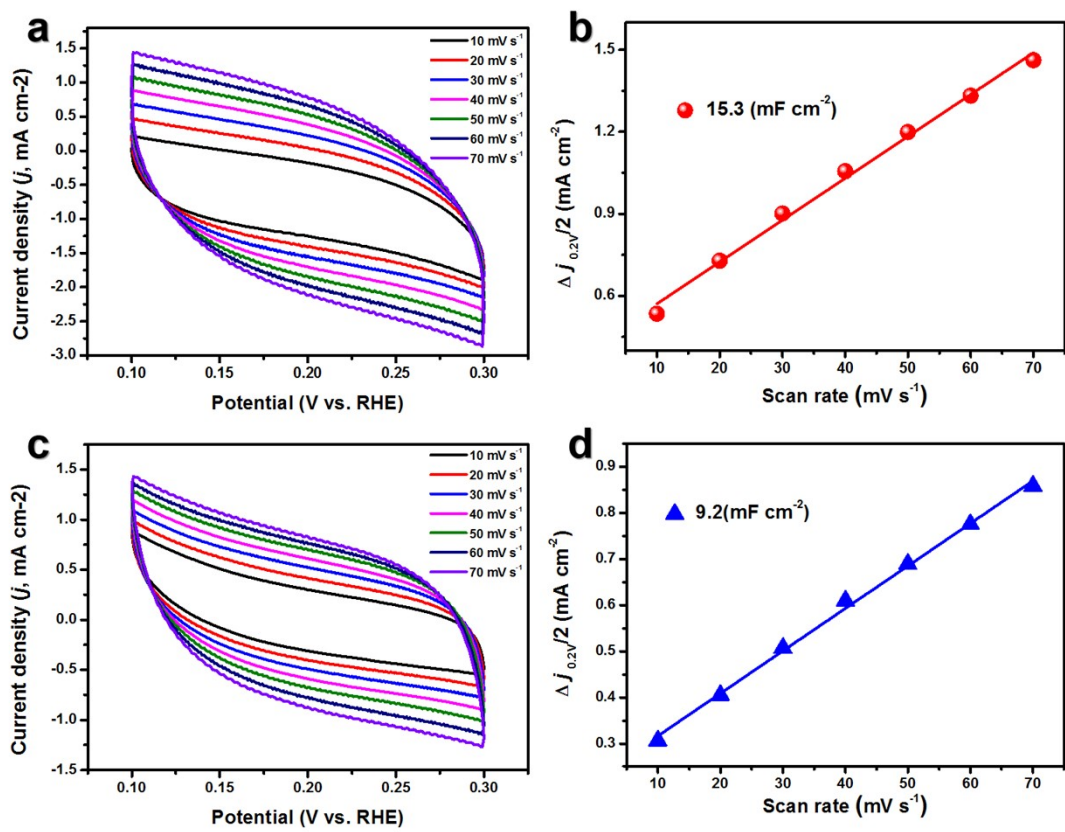


Fig. S6. Electrochemical double-layer capacitance (C_{dl}) measurements at different scanning rates of 10-70 mV s⁻¹ for (a, b) Fe-SnS₂/CC and (c, d) SnS₂/CC.

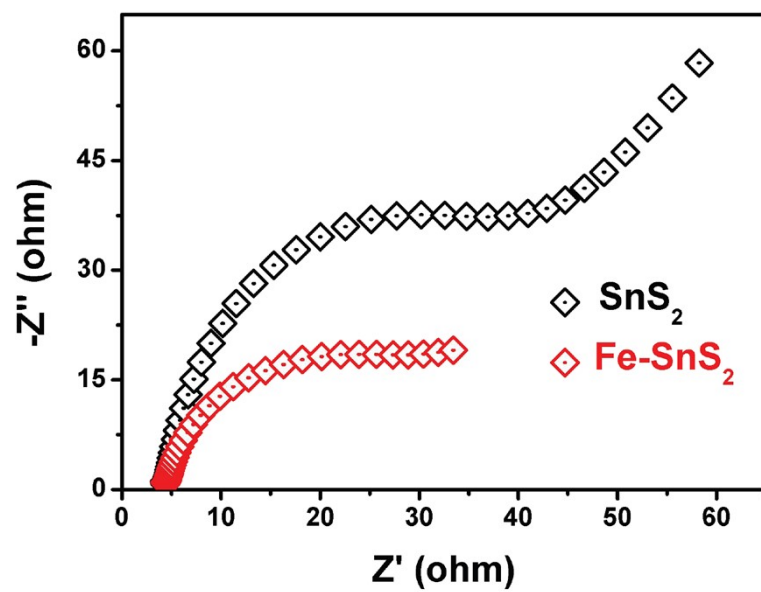


Fig. S7. Electrochemical impedance spectra of $\text{Fe-SnS}_2/\text{CC}$ and SnS_2/CC .

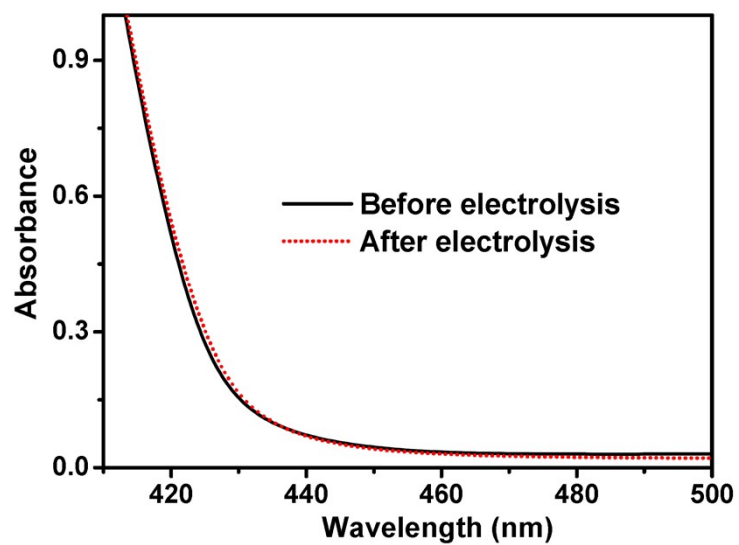


Fig. S8. UV-vis absorption spectra of before and after electrolysis for calculation of N_2H_4 concentration.

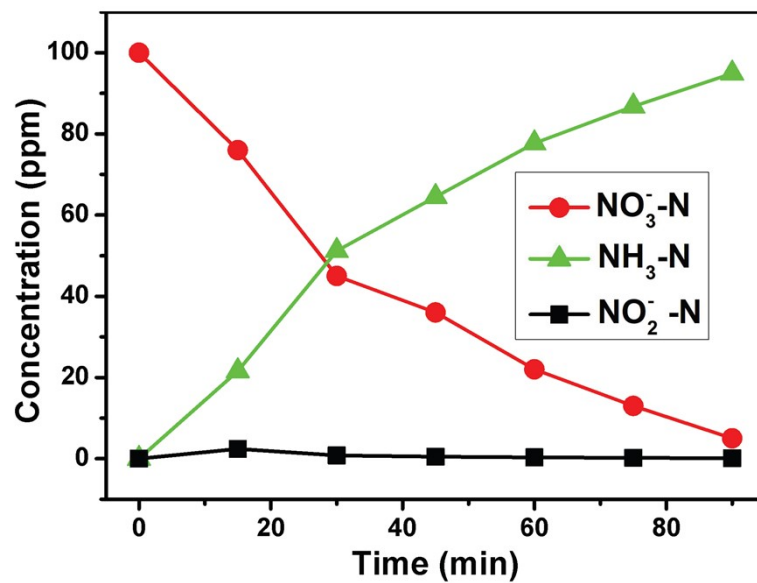


Fig. S9. The concentration of NO_3^- -N, NH_3 -N and NO_2^- -N in the electrolyte during the electrolysis at -0.7 V.

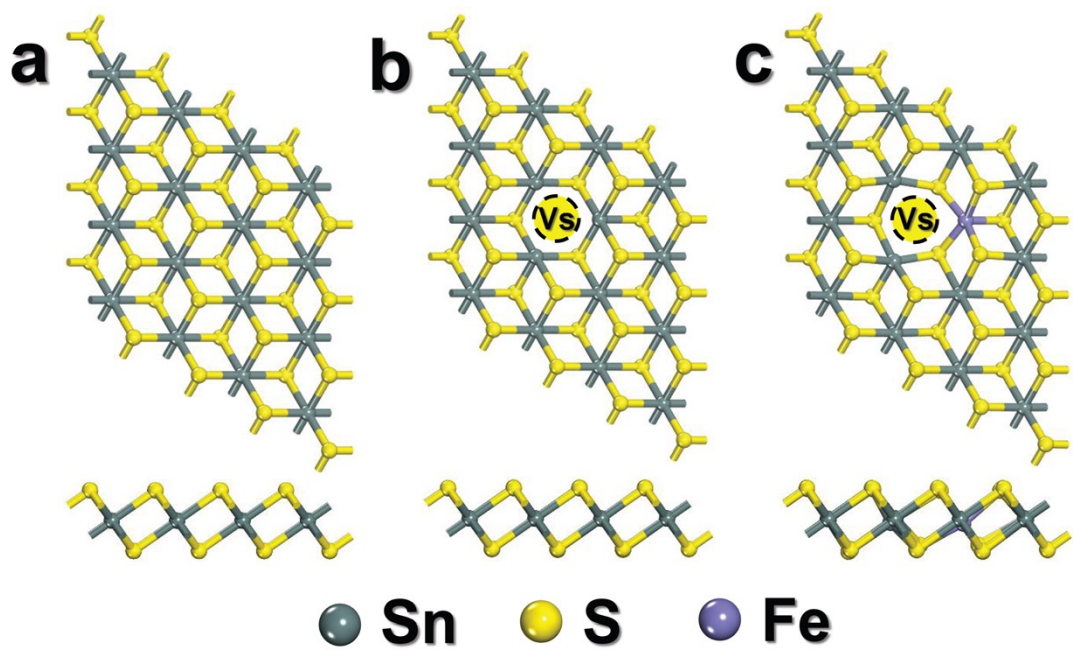


Fig. S10. Optimized structures of (a) SnS₂, (b) SnS₂-Vs and (c) Fe-SnS₂-Vs.

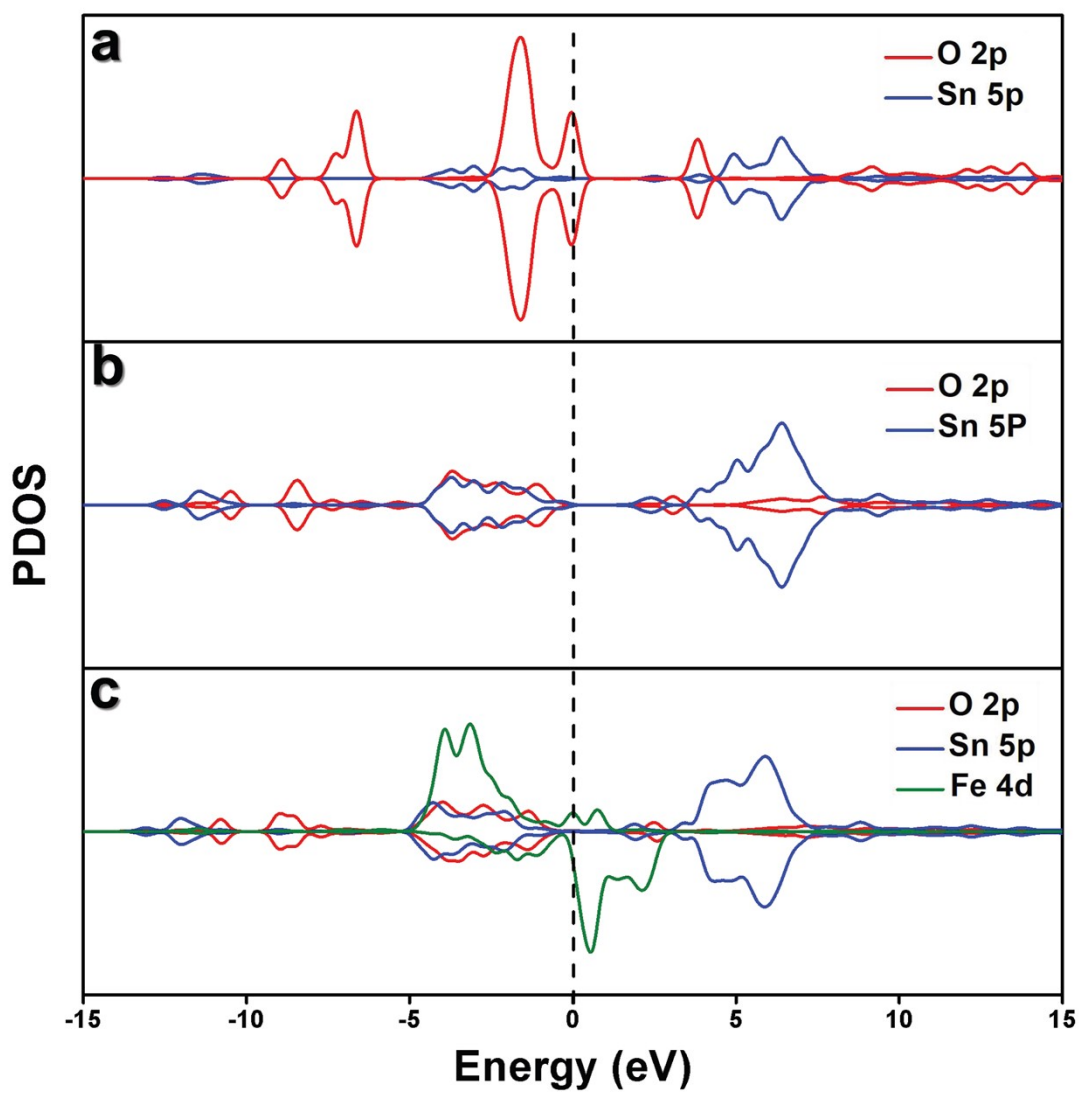


Fig. S11. PDOS of (a) SnS₂, (b) SnS₂-Vs and (c) Fe-SnS₂-Vs.

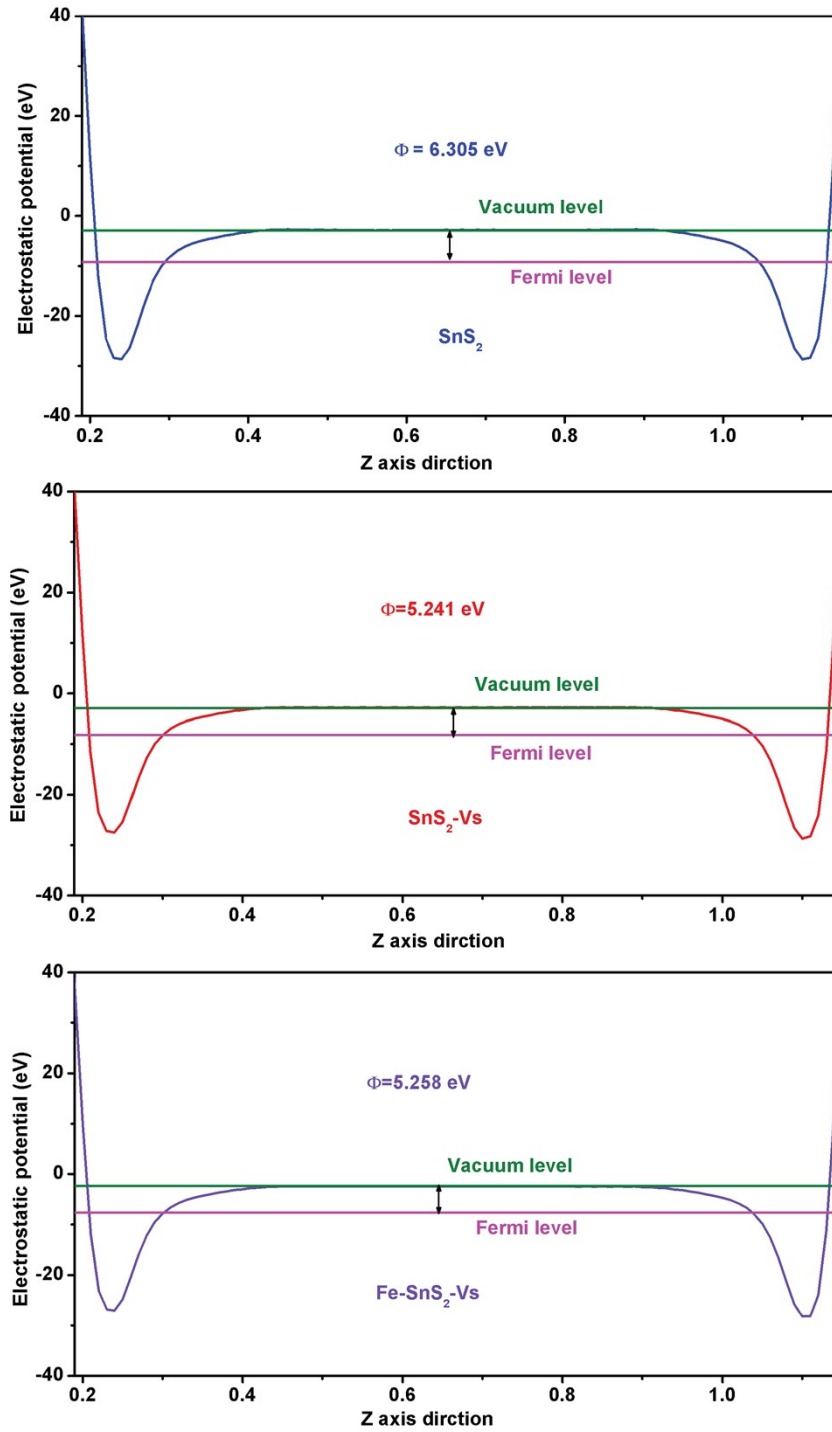


Fig. S12. Average potential profiles along c-axis direction for calculating the work functions of (a) SnS_2 , (b) $\text{SnS}_2\text{-Vs}$ and (c) $\text{Fe-SnS}_2\text{-Vs}$.

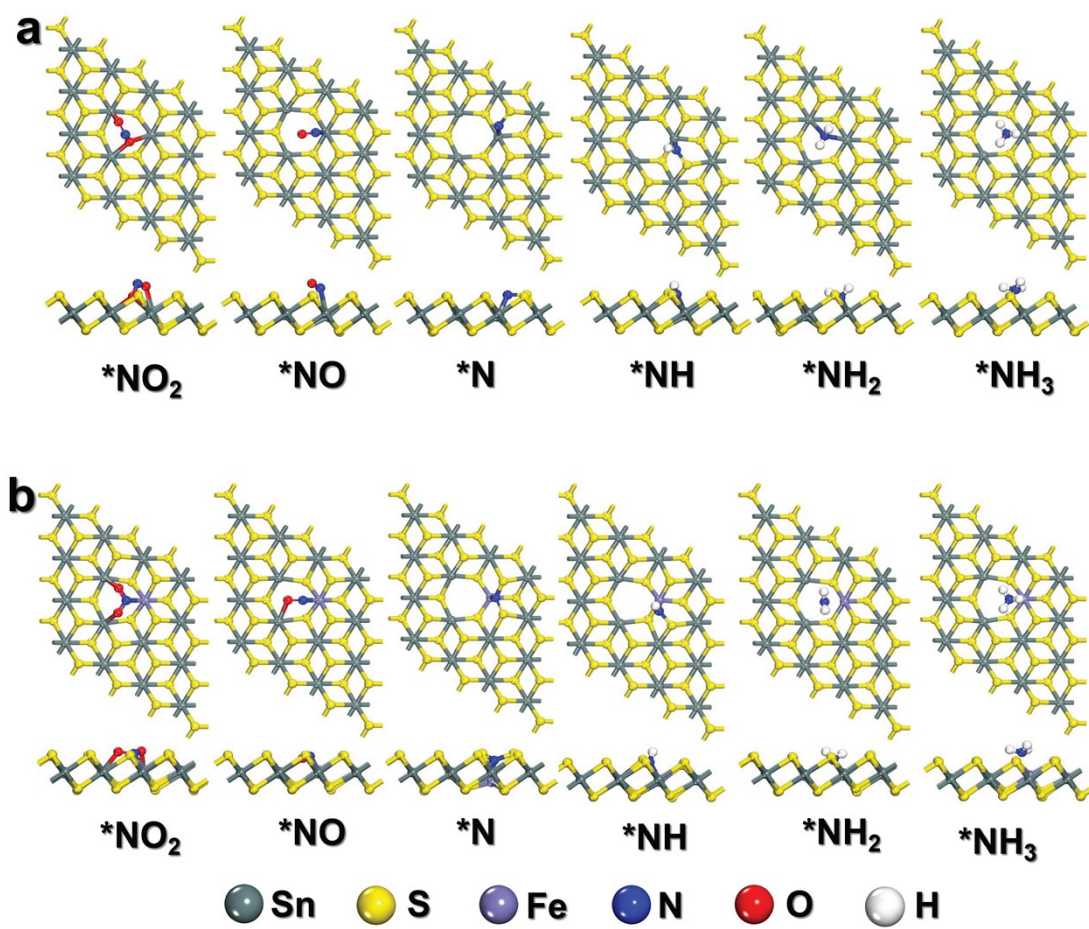


Fig. S13. Top and side view adsorption configurations of NO₂RR intermediates on (a) SnS₂-Vs and (b) Fe-SnS₂-Vs.

Table S1. Comparison of optimum NH₃ yield and Faradic efficiency (FE) for recently reported state-of-the-art NO₃RR electrocatalysts at ambient conditions.

| Catalyst | Electrolyte | NH ₃ yield rate & Optimum Potential (V vs RHE) | FE & Optimum Potential (V vs RHE) | Ref. |
|--|--|--|--|------------------|
| Fe ₃ O ₄ /SS | 0.1 M NaOH (0.1 M NaNO ₃) | 10.15 mg h ⁻¹ ·cm ⁻² @-0.5 | 91.5%@-0.5 | 7 |
| Co ₂ AlO ₄ /CC | 0.1 M PBS (0.1 M NO ₃ ⁻) | 7.9 mg h ⁻¹ cm ⁻² @-0.7 | 92.6%@-0.7 | 8 |
| ZnCo ₂ O ₄ NSA/CC | 0.1 M NaOH (0.1 M NaNO ₃) | 10.79 mg h ⁻¹ cm ⁻² @-0.8 | 98.33%@-0.6 | 9 |
| Cu-PTCDA | 1 M PBS (500 ppm KNO ₃) | 0.44 mg h ⁻¹ cm ⁻² @-0.4 | 77 ± 3%@-0.4 | 10 |
| CuCl BEF | 0.5 M Na ₂ SO ₄ (100 mg/LNO ₃ ⁻) | 1.82mg h ⁻¹ cm ⁻² @-1.0 | 88%@-1.0 | 11 |
| Poly-Cu ₁₄ cba | 0.5 M K ₂ SO ₄ (250 ppm NO ₃ ⁻) | 0.17 mg h ⁻¹ cm ⁻² @-1.15 | 90%@-1.05 | 12 |
| CuO NWAs | 0.5 M Na ₂ SO ₄ (200 ppm NO ₃ ⁻) | 4.16 mg h ⁻¹ cm ⁻² @-0.85 | 95.8%@-0.85 | 13 |
| CF@Cu ₂ O | 0.1 M PBS (0.1 M NaNO ₂) | 7.51 mg h ⁻¹ cm ⁻² @-0.6 | 94.21%@-0.6 | 14 |
| Pd facets | 1 M NaOH (20 mM NO ₃ ⁻) | 0.31 mg h ⁻¹ cm ⁻² @-0.2 | 35%@-0.2 | 15 |
| Fe-SnS₂/CC | 0.5 M Na₂SO₄ (0.1 M NaNO₃) | 7.2 mg h⁻¹ cm⁻²@-0.8 | 85.6%@-0.7 | This work |

Supplementary references

1. D. Zhu, L. Zhang, R. E. Ruther and R. J. J. N. m. Hamers, *Nat. Mater.*, 2013, **12**, 836-841.
2. Y. Wang, C. Wang, M. Li, Y. Yu and B. Zhang, *Chem. Soc. Rev.*, 2021, **50**, 6720-6733.
3. L. C. Green, D. A. Wagner, J. Glogowski, P. L. Skipper, J. S. Wishnok and S. R. J. A. b. Tannenbaum, *Anal. Biochem.*, 1982, **126**, 131-138.
4. G. W. Watt and J. D. Chrisp, *Anal. Chem.*, 1952, **24**, 2006-2008.
5. Y. Guo, R. Zhang, S. Zhang, Y. Zhao, Q. Yang, Z. Huang, B. Dong, C. J. E. Zhi and E. Science, *Energy Environ. Sci.*, 2021, **14**, 3938-3944.
6. A. A. Peterson, F. Abild-Pedersen, F. Studt, J. Rossmeisl, J. K. J. E. Nørskov and E. Science, *Energy Environ. Sci.*, 2010, **3**, 1311-1315.
7. X. Fan, L. Xie, J. Liang, Y. Ren, L. Zhang, L. Yue, T. Li, Y. Luo, N. Li, B. Tang, Y. Liu, S. Gao, A. A. Alshehri, Q. Liu, Q. Kong and X. Sun, *Nano Res.*, 2021, **15**, 3050-3055.
8. Z. Deng, J. Liang, Q. Liu, C. Ma, L. Xie, L. Yue, Y. Ren, T. Li, Y. Luo and N. J. C. E. J. Li, *Chem. Eng. J.*, 2022, **435**, 135104.
9. Z. Li, J. Liang, Q. Liu, L. Xie, L. Zhang, Y. Ren, L. Yue, N. Li, B. Tang and A. A. Alshehri, *Mater. Today Phys.*, 2022, **23**, 100619.
10. G.-F. Chen, Y. Yuan, H. Jiang, S.-Y. Ren, L.-X. Ding, L. Ma, T. Wu, J. Lu and H. Wang, *Nat. Energy*, 2020, **5**, 605-613.
11. W. J. Sun, H. Q. Ji, L. X. Li, H. Y. Zhang, Z. K. Wang, J. H. He and J. M. A. C. I. E. Lu, *Angew. Chem. Int. Ed.*, 2021, **60**, 22933-22939.
12. Y.-M. Wang, J.-M. Cai, Q.-Y. Wang, Y. Li, Z. Han, S. Li, C.-H. Gong, S. Wang, S.-Q. Zang and T. C. W. Mak, *Angew. Chem. Int. Ed.*, 2022, **134**, e202114538.
13. Y. Wang, W. Zhou, R. Jia, Y. Yu and B. Zhang, *Angew. Chem. Int. Ed.*, 2020, **59**, 5350-5354.
14. Q. Chen, X. An, Q. Liu, X. Wu, L. Xie, J. Zhang, W. Yao, M. S. Hamdy, Q. Kong and X. Sun, *Chem. Commun.*, 2022, **58**, 517-520.
15. J. Lim, C.-Y. Liu, J. Park, Y.-H. Liu, T. P. Senftle, S. W. Lee and M. C. Hatzell, *ACS Catal.*, 2021, **11**, 7568-7577.